Grasp Planning Pipeline for Robust Manipulation of 3D Deformable Objects with Industrial Robotic Hand + Arm Systems

Lazher Zaidi, Juan Antonio Corrales Ramon, Laurent Sabourin, Belhassen-Chedli Bouzgarrou, Youcef Mezouar

applied sciences

MDPI

Article

Grasp Planning Pipeline for Robust Manipulation of 3D Deformable Objects with Industrial Robotic Hand + Arm Systems

Lazher Zaidi [1,*], Juan Antonio Corrales Ramon [2], Laurent Sabourin [2], Belhassen Chedli Bouzgarrou [2], and Youcef Mezouar [2]

[1] LINEACT Laboratory, EA 7527, CESI ROUEN, 76800 Saint-Étienne-du-Rouvray, France
[2] Université Clermont Auvergne, CNRS, SIGMA Clermont, Institut Pascal, F-63000 Clermont-Ferrand, France; juan.corrales@sigma-clermont.fr (J.A.C.R.); Laurent.Sabourin@sigma-clermont.fr (L.S.); chedli.bouzgarrou@sigma-clermont.fr (B.C.B.); youcef.mezouar@sigma-clermont.fr (Y.M.)
* Correspondence: lzaidi@cesi.fr (L.Z.)

Received: 17 October 2020; Accepted: 30 November 2020; Published: date

Abstract: In the grasping and manipulation of 3D deformable objects by robotic hands, the physical contact constraints between the fingers and the object have to be considered in order to validate the robustness of the task. Nevertheless, previous works rarely establish contact interaction models based on these constraints that enable the precise control of forces and deformations during the grasping process. This paper considers all steps of the grasping process of deformable objects in order to implement a complete grasp planning pipeline by computing the initial contact points (pregrasp strategy), and later, the contact forces and local deformations of the contact regions while the fingers close over the grasped object (grasp strategy). The deformable object behavior is modeled using a nonlinear isotropic mass-spring system, which is able to produce potential deformation. By combining both models (the contact interaction and the object deformation) in a simulation process, a new grasp planning method is proposed in order to guarantee the stability of the 3D grasped deformable object. Experimental grasping experiments of several 3D deformable objects with a Barrett hand (3-fingered) and a 6-DOF industrial robotic arm are executed. Not only will the final stable grasp configuration of the hand + object system be obtained, but an arm + hand approaching strategy (pregrasp) will also be computed.

Keywords: 3D deformable object; grasping; robust manipulation; robot hand

1. Introduction

Nowadays, manipulation has become an increasingly important standing research topic in robotics. Most of the related works in this field consider the grasping of rigid bodies as an extensively studied area, which is rich with theoretical analysis and implementations using different robotic hands ([1–8]). Robotic grasping of deformable objects has also acquired importance recently due to several potential applications in various areas, including biomedical processing, the food processing industry, service robotics, robotized surgery, etc. ([9–14]). Recent surveys covering the literature related to the robotic grasping and manipulation of deformable objects can be found in [12,15].

Nevertheless, efficient and precise (i.e., deformation/force control) robotic grasping of 3D deformable objects remains an underdeveloped area within the robotics community due to the technical and methodological difficulties of the problem. In fact, this problem involves implementing two main steps with their own subproblems: determining the initial location of the grasp points and moving the hand + arm system towards them (i.e., pregrasping strategy), and closing the fingers of the robotic hand

until a robust grasp is reached while taking into account the deformation of the object (i.e., grasping strategy).

In the case of the pregrasp strategies, two main problems arise: firstly, implementing a grasp quality measure to choose the most stable grasp configuration; secondly, applying the kinematic constraints of the hand + arm system so that the chosen grasp is reachable. Several previous surveys to quantify grasp quality were developed in [1,16–19]. All of these approaches have studied stable grasps and developed various stability criteria to find optimal grasps for rigid objects. Nevertheless, the development of algorithms that can efficiently synthesize grasps in 3D deformable objects is still a challenging research problem. Wakamatsu et al. [20] analyzed the stable grasping of deformable objects based on extending the concept of force closure of rigid objects to deformable planar objects with bounded applied forces. Mira et al. [21] presented a grasp planner that can reproduce the actions of a human hand to determine the contact points. Their algorithm combines the position information of the hand with visual and tactile data in order to achieve a hand–object configuration. This method is applied to planar objects without considering applied forces by fingers and object deformation. Xu et al. [22] proposed a grasp quality metric for hollow plastic objects based on minimal work in order to combine wrench resistance and object deformation. Jorgensen et al. [23] presented a generic solution for doing pick and place operations of meat pieces with a vacuum gripper. This solution used a grasp quality metric that combines wrench resistance and object deformation. It was based on the computation of the required work to resist an external wrench and it can only be applied to planar objects, without a direct relation between applied forces and deformation. In fact, none of these works can be applied to general 3D deformable objects and they are solutions for specific types of objects.

For the second step of the grasping problem (i.e., closing of the fingers), previous grasping synthesis methods are mainly based on the generation of force closure (FC) grasps ([24–26]). This means that the robotic hand is able to maintain the manipulated object inside the palm despite any external disturbance and evaluate the contact forces including those due to friction. FC is generally used to implement the grasping of rigid objects with a low number of frictional contacts by taking into account geometric criteria of their contact surfaces. Nevertheless, traditional FC-based approaches cannot be applied to deformable objects due the complexity of their interaction with the robotic hand's fingers: the object deforms (i.e., its size and shape are changed) and the contact surfaces evolve dynamically while contact forces are applied by the fingers. New reactive methods based on the detection and avoidance of slippage have been developed in order to solve this limitation in the grasping of deformable objects. For instance, Kaboli et al. [27] computed the tangential forces required for slippage avoidance and adjusted the fingers' relative positions and grasping forces accordingly, taking into account an estimation of the weight of the grasped object. The main drawback of this approach is that the relationship between applied forces and object deformation is not considered. Zhao et al. [28] proposed a new slip detection sensor based on video processing in order to perceive multidimensional information, including absolute slip displacement, the deformation at the object surface, and force information. This method is only applied for 2D objects with transparent and reflective surface, such as pure glass. However, these types of materials are not common in deformable objects. In addition, the stress state of the gripper–object interface is not precisely analyzed when taking into account the properties of the object's material.

In order to solve all these limitations of reactive strategies, it is crucial to use a suitable contact model ([29–32]) that explains the coupling between the contact forces and the object deformations. A precise contact model can be exploited to provide a set of grasping forces and torques that can be applied to maintain equilibrium before and after the deformation [33]. Thereby, the grasp stability can be computed in real-time while the contact surfaces evolve during deformation. This evolution of the object surface is obtained by sampling mechanical deformation models [34], mainly mass-spring systems ([35,36]), finite element methods (FEM) ([37,38]), and impulse-based methods ([39]). The mass-spring system is a fast and interactive physical model with a solid mathematical foundation and well-understood dynamics. This model provides a more realistic

force/deformation behavior in the case of large deformations, while maintaining the capability of real-time response. FEM provides higher accuracy, but it requires higher numerical computation, which is more appropriate for offline simulations. Therefore, this paper uses a deformation model based on nonlinear mass-spring elements distributed across a tetrahedral mesh: lumped masses are attached to the nodes and nonlinear springs represent the edges. The tracking of the mesh nodes positions is assured by solving a dynamic equation based on Newton's second law. The main interests of this deformation model are the dynamic predictions of the object's deformations and its realistic behavior, which results from the nonlinearity of the object. More details about this object deformation model can be found in previous works [40] and it will be used by the new proposed grasp synthesis algorithm.

Several previous works have taken into account the deformation of soft objects while grasping them without integrating precise contact interaction models. Berenson et al. [41] presented a vision-based deformation controller for elastic planar objects without considering the grasp properties. This method takes into account just one contact point which cannot be used with a multifingered hand for grasping deformable objects. Similarly, Nadon et al. presented a model-free algorithm in [42] based on visual information for automatically selecting the contact points between the fingers and the object's contour in order to control its shape. However, contact forces and object stability were not considered. Grasping deformable planar objects using contact analysis was proposed in [43]. It was based on an algorithm to track the contact regions during the squeezing process and determine the stick/slip mode in the contact area. Fingers' displacements were considered rather than forces, and object stability was not guaranteed. Similarly, Sanchez et al. [44] developed a manipulation pipeline that is able to estimate and control the shape of a deformable object with tactile information but the stability of the grasp is not considered. Authors in [45] proposed a new approach to lift a deformable 3D object, causing small deformations of the object by employing two rigid fingers with contact friction. This approach considered small deformations within the scope of the linear elasticity during the grasp operation and did not deal with the nonlinear relationships between deformations and forces of 3D soft objects. Jorgensen et al. [46] presented a simulation framework for using machine learning techniques to grasp deformable objects. In this framework, robot motions were parameterized in terms of grasp points, robot trajectory, and robot speed. Hu et al. [47] presented a general approach to automatically handle soft objects using a dual-arm robot. An online Gaussian process regression model was used to estimate the deformation function of the manipulated objects and low-dimension features described the object's configuration. Finally, new works (such as [48,49]) integrate deep-learning techniques, 3D vision, and tactile information in order to fold/unfold and pick-and-place clothes. Although all these works consider the deformation of the object while manipulating it, an initial stable grasp is supposed to be known and nonlinear force–deformation relations are not computed during the handling process.

None of these works combine all the previously explained elements that are required for the implementation of a general and complete grasp planning pipeline for 3D deformable objects: a pregrasp strategy for reaching the object that takes into account grasp quality metrics for 3D deformable objects, and a grasp strategy for closing the fingers that guarantees a stable configuration of the object by considering its deformation and the applied contact forces. This paper involves an extension of our previous grasping strategy in [33] in order to implement this complete grasp planning pipeline. Firstly, we adapt the stability criteria developed for robotic grasp synthesis of rigid objects to 3D deformable objects (see Section 2 for a general description of the strategy and Section 3 for the new geometric criterion of the initial grasp). We also defined a new pregrasp strategy (Sections 4 and 5) in order to approach the deformable objects in an optimal way before manipulating them by using the previous grasping metrics. This grasping strategy is based on an interaction model developed by the authors in a previous work [40]. Section 6 indicates how this finger–object contact model is used in order to compute the contact forces to be applied by the fingers for a stable grasp of the deformable object and what their precise values are in the proposed experiments. We consider the problem of grasping and manipulation of a 3D isotropic deformable objects with a 3-fingered Barrett hand. This hand is installed as the end-effector of a 6-DOF Adept Viper robotic arm S1700D. Finally, a complete grasping planning

strategy combining the pregrasp and grasp synthesis strategies of the hand + arm system is developed and tested with real objects (Section 7).

2. General Description of the Grasp Planning Pipeline

As indicated in the introduction section, by using our previously developed contact model [33], we can handle highly deformable objects and give precise estimations of the contact forces generated while deforming them. Those precise estimations would guarantee the static equilibrium of the object by considering new grasps metrics (Section 3) and optimizing the pregrasp configuration of the robotic hand around the object (Sections 4 and 5).

The flowchart in Figure 1 shows all the steps that are required in order to compute and execute a robust grasp (i.e., the configuration of fingers over the surface of the object) that guarantees the stability of the object with our grasp planning pipeline.

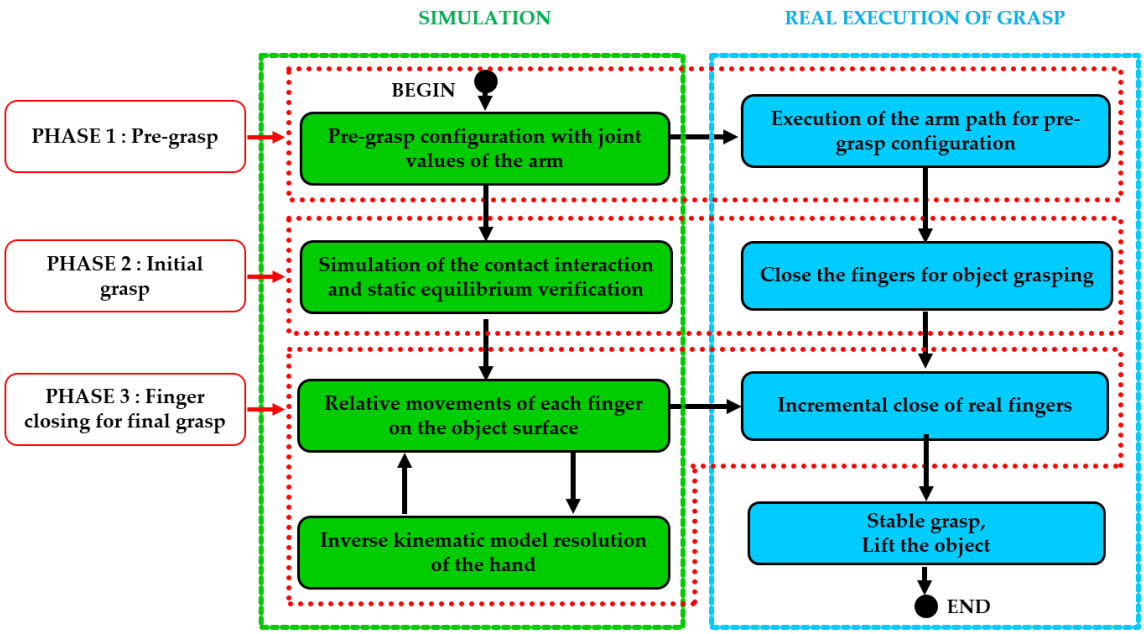

Figure 1. Flowchart of the proposed grasp planning pipeline (i.e., pregrasp and grasping strategies) for handling deformable objects with a hand + arm robot system.

In order to execute the computed grasp, the first step determines the pregrasp configuration. In fact, the complete grasp planning strategy is divided into two phases: First, determining the configuration of the robotic arm to bring the hand close to the object so that the fingers of the hand can reach the surface of the object (Section 5). The second phase is determining the appropriate initial configuration of the fingers of the hand to grasp the object based on a new geometric criterion (Sections 3 and 4). The determination of the joint parameters of the arm and the hand for executing both phases is ensured by the resolution of their inverse kinematics (IK).

Once the pregrasp step is performed, the robot moves next to the object and the fingers reach the initial grasp. No important deformation is supposed to be generated when the fingers come into contact with the object since a very small contact force will be firstly applied in order to avoid that the grasp location changes. As soon as this initial grasp is executed precisely, the third step of the algorithm is activated and an iterative closing of the fingers begins, based on the simulation of the contact interaction model (Section 6). At each iteration of the simulation, the deformations of the object are updated and the generated contact forces are computed. The computed contact forces are used to evaluate the static equilibrium of the object + fingers system. The iterative process is repeated in simulation until the static equilibrium is reached (see all these steps in simulation on the left side of the flowchart in Figure 1).

Upon completion of the simulation process, the real handling and manipulation of the object can be performed by executing the contact forces obtained from simulation (see steps on the right side of the flowchart). Firstly, the object is installed at the workspace of the robot with the same relative configuration as at the beginning of the simulation. Then, the robotic arm moves towards the pregrasp configuration (i.e., phase 1 in reality) and the hand fingers are moved towards the initial contact points by position control (i.e., phase 2 in reality). At this stage (beginning of phase 3 in reality), the fingers are closed by force control and apply progressive squeezing of the object until the contact forces (which are measured by contact sensors installed inside each finger of the Barrett hand) become equal to the contact forces computed at the simulation step. These contact forces guarantee the equilibrium of the object–hand system (as validated by the simulation). Thereby, the object can be lifted up from the table without any risk of sliding and can be robustly manipulated. In the next sections, all these steps are described in detail and are validated with real pick-and-place experiments of deformable objects by a hand + arm robot system (Section 7).

3. Synthesis of the Initial Grasp Configuration

In this section, we address the characterization of the object stability for a three-fingered grasp. This implies determining a force closure configuration based on the choice of three contact points from the set of all the points representing the outer 3D surface of the object. The following assumptions are considered in this procedure:

- The use of three fingers for the grasp operation modeled as hemispheres with radius R.
- The first contacts between the fingers and the object are point contacts.
- The outer surface of the object is represented by a set of points Ω, which are described by their position vectors $\vec{P_i}$ measured with respect to a reference frame located at the center of mass ($\vec{P_{co}}$) of the object.

In fact, a 3-fingered grasp is more reliable in terms of stability, slip avoidance, and balance of forces when it converges towards an ideal equilateral grasp [17]. Thus, each three-fingered grasp can be characterized by a value which represents its similarity to an equilateral triangle. We suggest an algorithm based on geometric criteria to find this equilateral grasp. This algorithm determines, at first, the set of all possible grasping triangles by scanning the points belonging to the contact surface Ω. Then, using the Q_1 criterion presented by Roa [17], our algorithm compares the angle values (alpha, beta, and lambda) of these triangles with $\pi/3$ (i.e., the angle that characterizes an equilateral triangle) in order to choose the configuration closest to an equilateral triangle (see Figure 2):

$$Q_1 = \frac{3}{2\pi}\left(\left|\alpha - \frac{\pi}{3}\right| + \left|\beta - \frac{\pi}{3}\right| + \left|\gamma - \frac{\pi}{3}\right|\right). \quad (1)$$

For a target angle value of $3/2\pi$, the minimum possible value of Q_1 is 0 for a perfect equilateral triangle, 2 for the most unfavorable case (the triangle degenerates into a segment), and 1 for an intermediate state.

For evaluating the angles of the triangle, we use a margin of error defined by the interval [0, 0.3]. Depending on the density of the points of the contact surface Ω, this algorithm can give several grasp configurations. Finally, a second criterion, referred to as Q_2, is used in order to choose one between them. It measures the distance between the center of the mass of the object C_O and the center of the grasping triangle C_T (Figure 3), defined as

$$Q_2 = |C_O - C_T|. \quad (2)$$

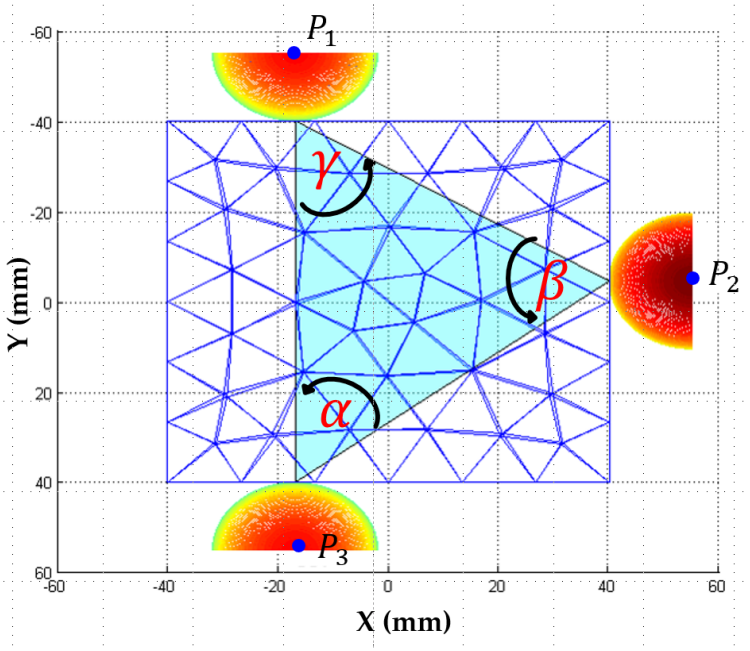

Figure 2. Force arrangement criteria.

This criterion was developed to obtain stable grasps with respect to the torques generated by gravitational and inertial forces [17]. The complete grasp synthesis algorithm based on the these two criteria Q_1 and Q_2 is represented in the diagram "Algorithm 1":

Algorithm 1 Synthesis of the 3 contact points for initial grasp configuration.

Grasp synthesis algorithm. Input: points P_i on contact surfaces Ω with their 3D coordinates

1. Calculation of the set Γ of grasp triangles defined from points P_i.
2. Calculation of the value of the angles of the grasp triangles of the set Γ.
3. Choice of the grasp triangles closer to an equilateral triangle by applying criterion Q_1, the set of these triangles is named Ψ.
4. Calculation of the barycenter C_T of the grasp triangles of the set Ψ.
5. Calculation of the distance between C_O and the centers C_T of the triangles of the set Ψ by applying criterion Q_2.
6. Choosing the triangle that minimizes Q_2.

Output: 3 initial contact points of the grasp configuration

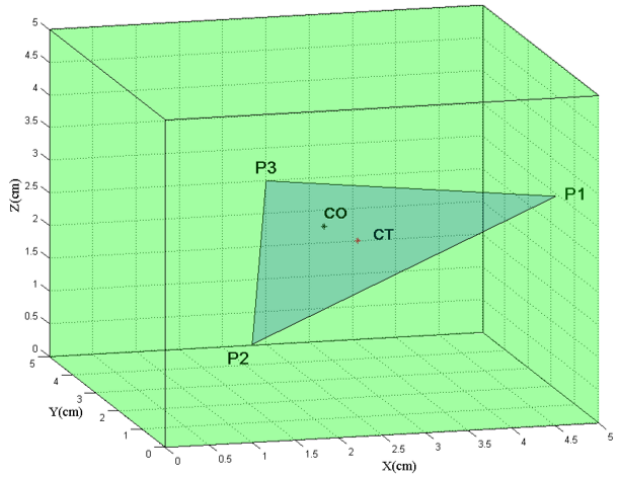

Figure 3. The distance between C_O and C_T.

4. Pregrasp Strategy for the Robotic Hand: Placement of the Fingers

In this section, we present the pregrasp strategy for reaching the three contact points of the initial grasp computed in Section 3 with a three-fingered robotic hand (e.g., the Barrett hand [50] in our experiments). In order to describe the kinematic model of the Barrett hand, we establish the joint frames of Figure 4. The movement of the fingers of the Barrett hand is controlled by defining 4 encoder values $[q_{M1} \dots q_{M4}]$ that are connected to the joint values φ_i of the fingers (Figure 4) by the following coupling relationships:

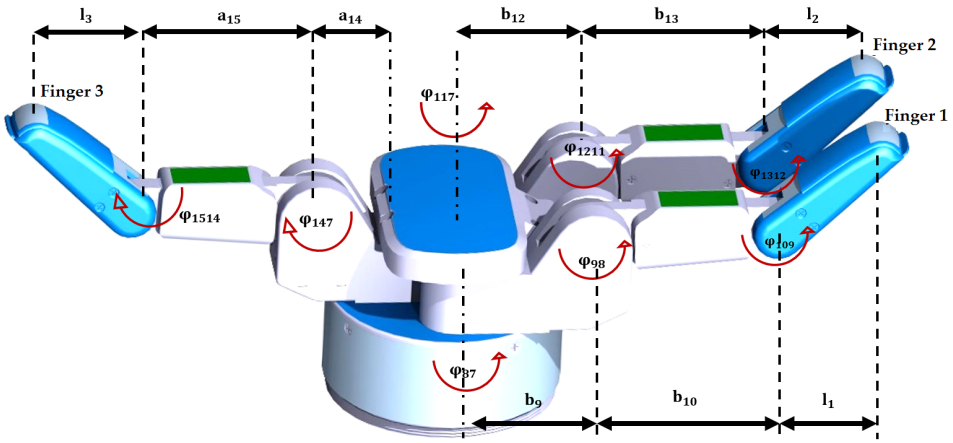

Figure 4. Barrett hand: dimensions, frames, and joints.

$$\begin{bmatrix} \phi_{98} \\ \phi_{109} \\ \phi_{1211} \\ \phi_{1312} \\ \phi_{147} \\ \phi_{1514} \\ \phi_{87} \\ \phi_{117} \end{bmatrix} = \begin{bmatrix} 1/125 & 0 & 0 & 0 \\ 1/375 & 0 & 0 & 0 \\ 0 & 1/125 & 0 & 0 \\ 0 & 1/375 & 0 & 0 \\ 0 & 0 & 1/125 & 0 \\ 0 & 0 & 1/375 & 0 \\ 0 & 0 & 0 & 2/35 \\ 0 & 0 & 0 & -2/35 \end{bmatrix} * \begin{bmatrix} q_{M1} \\ q_{M2} \\ q_{M3} \\ q_{M4} \end{bmatrix}, \tag{3}$$

where $q_{Mk} = \begin{bmatrix} 0 & 17,500 \end{bmatrix}$ for $k = \begin{bmatrix} 1 & 2 & 3 \end{bmatrix}$ (i.e., the range of variation of the encoders of the motors for closing/opening the three fingers), and $q_{M4} = \begin{bmatrix} 0 & 3150 \end{bmatrix}$ (i.e., the range of variation of the encoder of the motor 4 for separating fingers 1 and 2 around the palm).

The pregrasp strategy for the three-fingered robotic hand involves two steps: the first one aligns the orientation of the hand with the initial grasping triangle computed in Section 3; the second one adjusts this initial estimation of the grasp by taking into consideration the kinematic constraints of the hand. The first step consists of orientating the hand so that the TCP (Tool Center Point, defined along the axis perpendicular to the palm of the hand) coincides with the C_T grasp triangle center (as shown in Figure 5). The second step involves the resolution of the IK of the fingers in order to estimate the joint values to reach the three grasp points (P_1, P_2, and P_3) of the initial grasp triangle. If no IK solution is found, the length of the TCP line is changed and the IK resolution is recomputed. When an IK solution is found, the motor commands q_{Mk} are computed in order to attend to these joint values, by applying the inverse expression of (3). The implemented algorithm is shown in the diagram "Algorithm 2". In the context of this iterative solution search, we consider that the solution is validated for a value of joint angle difference for each of the fingers smaller than 2 degrees.

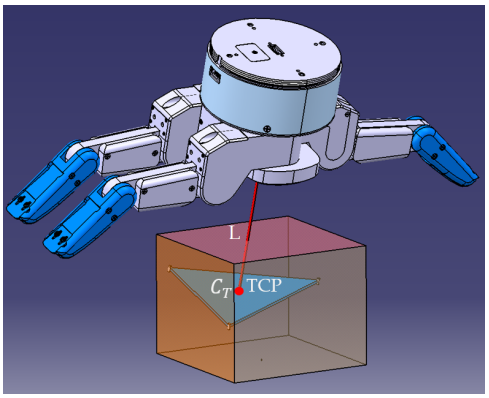

Figure 5. Intersection of the hand's Tool Center Point (TCP) with the center C_T of the grasp triangle.

Algorithm 2 Pregrasp strategy for the robotic hand.

Finger placement algorithm for the initial grasp. Input: grasp triangle computed by Algorithm 1

1. Reorientation of the hand in the grasp plan and coincidence of TCP with C_T.
2. Calculation of IK and definition of finger joint values.
3. Searching for a solution for q_{M1}, q_{M2}, and q_{M3} by successive iteration over the length L in order to find a solution.
4. Reorientation of the hand around TCP and adjustment of the distance L to define a solution for q_{M4}.

Output: Definition of the values of $[q_{M1} \dots q_{M4}]$ and the 6 components (position + orientation) of the tool frame defining the hand's TCP.

5. Pregrasp Strategy for the Hand + Arm System: Reaching Trajectory by the Arm

After establishing the initial grasp points of the fingers (Section 3) and the corresponding pregrasp configuration of the hand around the object (Section 4), we should execute the latter by moving the hand with a robotic arm that carries it. Figure 6 shows the flowchart of the pregrasp strategy for the hand + arm system that uses the IK of the arm and the hand for achieving this initial grasp. For implementing this planning strategy, we have chosen a 6-DOF robotic arm (e.g., a Viper S1700D for our real experiments) so that the hand can attain any pose (position + orientation) in the space around the object. Initially, the object is resting on a table, modeled by a plane parallel to the XY plane of the arm base.

For performing this pregrasp strategy, we should represent the object pose (position $[x, y, z]$ in mm and orientation $[y, p, r]$ in ZYZ Euler angles) from its original *WobjO* frame (object mark) to the *WobjU* frame (user mark), known by the arm (see Figure 7). The TCP pose will also be represented firstly in the *WobjO* frame in order to easily define relative movements between the object and the hand. Later, it will be transformed into the arm frame (*WobjU*) so that final movements of the arm can be computed.

Firstly, we want to reach the relative object + hand configuration of Figure 8, which consists of putting the TCP in coincidence with C_0 (see Figure 9b). Then, we use the results from Section 3 to determine the contact points. We calculate the grasp triangle formed by these three contact points as well as its centroid C_T. Finally, we define the final pregrasp configuration (defined in Figure 5) by the translation and orientation of the hand. This step consists of matching the two TCP and C_T points and aligning the Z axis of the TCP coordinate system perpendicular to the grasp triangle (see Figure 9c) by computing the arm movements required to reach the tool frame obtained by Algorithm 2. When this final pregrasp configuration is reached by the hand, the fingers will be closed by applying the joints'

angles obtained with Algorithm 2. An example of the main execution steps of this pregrasp strategy for a cube is shown in Figure 9.

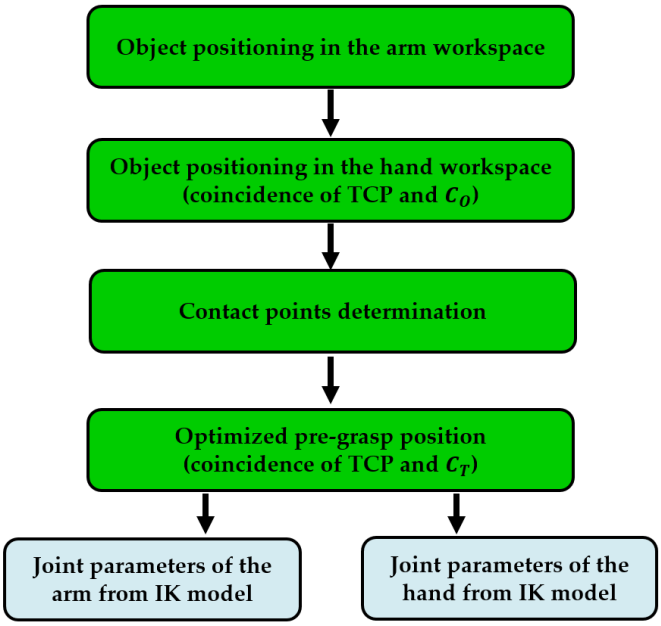

Figure 6. Flowchart for the pregrasp planning strategy of the hand + arm system. IK—Inverse Kinematics.

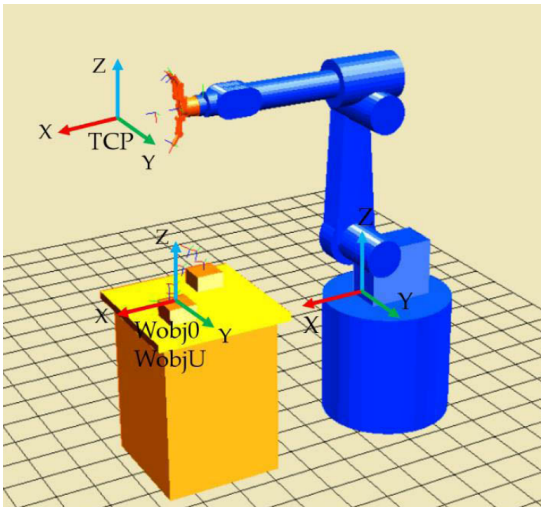

Figure 7. Main frames of the hand + arm system, simulated in Matlab.

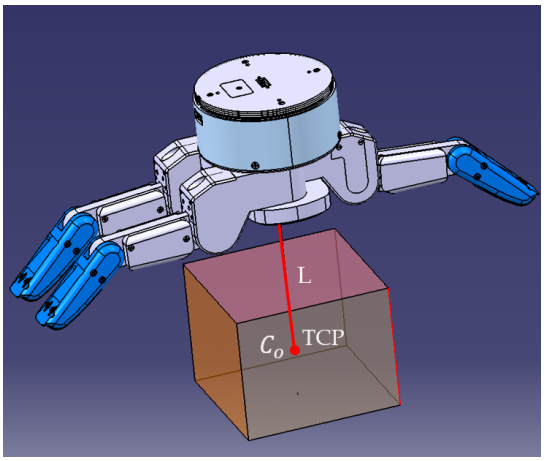

Figure 8. Intersection of TCP and C_0.

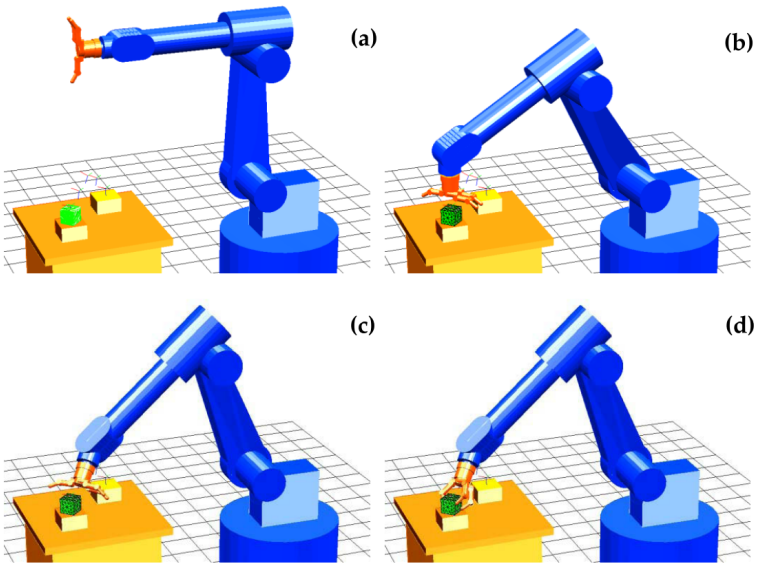

Figure 9. Main execution steps of the pregrasp strategy for the hand + arm system in order to grasp a cube: (**a**) initial robot–object configuration, (**b**) reaching trajectory (intersection of TCP and C_O), (**c**) hand orientation (intersection of TCP and C_T), (**d**) pregrasp configuration.

6. Final Stable Grasp Execution Based on Contact Interaction Modeling

In order to be able to evaluate the equilibrium with all the forces that take place in the real experiment while the fingers of the hand are closing, a model of the contact interactions between the fingertips and the object is required for precisely determining the forces–deformations relationship during grasping. This model will receive as input the initial grasp of the object without any deformation (i.e., the initial contact points of the fingertips over the object's surface or contact polygon determined at Section 3 and the fingers' configuration of the pregrasp strategy are described in Sections 4 and 5).

After this initial grasp, the fingers should close iteratively towards the center of the object until the equilibrium of all forces over the object is reached and a stable grasp is performed. With the aim of computing the required fingertip forces for this equilibrium, the simulation of this contact model is achieved in several sequential steps. Firstly, the contact between fingers and the object is detected. Secondly, contact forces are computed (by the evaluation of the relative velocity between the fingers and the object). Finally, the static equilibrium is checked for grasping stability. At each iteration of the simulation, the dynamic model updates the overall shape and contact area deformations due to the applied forces. Contact forces are individually calculated for each contact point, which gives a realistic distribution of the contact pressure in the contact zone. The contact model takes into account

the normal forces and the two modes of the tangential forces due to friction: slipping and sticking modes. As the object is modeled by a set of nonlinear spring–damper pairs, the nonlinear normal force is given by

$$f_{n_j} = \begin{cases} 0 & ,\delta_j \leq 0 \\ max(0, (K\delta_j^n + C\dot{\delta}_j)) & \end{cases} \tag{4}$$

$$\mathbf{f}_{n_j} = f_{n_j}\mathbf{n}_{fj}, \tag{5}$$

where δ_j is the penetration distance measured along the normal direction to the contact surface j; K and C are the contact stiffness and damping constants, respectively. Those parameters depend on Young's modulus and the Poisson ratios. Based on the work presented in the literature [51,52], the stiffness constant is calculated by

$$K = 2\Psi\sqrt{R}, \tag{6}$$

where Ψ is a constant, calculated according to the mechanical properties of the two objects in contact, and it is given by

$$\Psi = \frac{1}{\frac{1-v_1^2}{E_1} + \frac{1-v_2^2}{E_2}}, \tag{7}$$

where E_1 and E_2 are the Young's modulus; v_1 and v_2 are the Poisson ratios of the finger and the object, respectively. The damping constant is determined by

$$C = 4\pi R\gamma, \tag{8}$$

where γ is a constant.

To characterize these mechanical parameters, compression tests are done for obtaining curves of stress evolution according to compressive deformation (see [33] for photos and detailed results of this calibration process). Thereby, the Young's modulus (4.928 MPa) and the Poisson's ratio (0.39) of the material of the objects (i.e., foam) to be grasped during the real experiments in Section 7 are identified.

Modeling of the tangential force, acting along each contact, is required in order to prevent any slippage and to ensure grasp stability. The contact model takes into account the two modes of the tangential forces due to friction: slipping and sticking modes. In this model, a parallel spring–damper is attached to the ground at one end, via a slider element, and to the fingertip at the other end. Therefore, the contact point location dynamically changes in the slipping condition. These variables correspond to the relative displacements at the contact point due, respectively, to sticking and slipping. They are dynamically reset to zero if the contact is broken. The sliding friction force can be defined in terms of the Coulomb law as follows:

$$\mathbf{f}_{slip} = \begin{cases} 0, & \|\mathbf{V}_t\| = 0 \\ -\mu f_n \frac{\mathbf{V}_t}{\|\mathbf{V}_t\|} & \end{cases}, \tag{9}$$

where μ, f_n, and V_t are friction coefficient, normal force, and tangential velocity, respectively. With this model, the contact point location dynamically changes in the slipping condition. If the tangential force norm is less than the threshold of sliding, then we have a sticking mode whose tangential force is defined by

$$\mathbf{f}_{stick} = \begin{cases} 0, & v = 0 \\ -(k_t v - c_t \dot{v})\, \frac{\mathbf{P_c P_s}}{\|\mathbf{P_c P_s}\|}, & v > 0 \end{cases}, \tag{10}$$

where v is the tangential deformation at the contact facet, P_c is the contact point position, and P_s is the contact point position at the sticking regime. The parameters k_t and c_t are respectively tangential stiffness and damping coefficients estimated by using Dopico's method [30].

As indicated at the beginning of this section, this contact model will be executed after the initial grasp configuration (obtained as output of the pregrasp strategy) is reached and the fingers begin to

touch the surface of the object. In fact, a simulation of the grasping execution strategy is implemented in Matlab in order to determine the contact forces that should be applied to reach a robust grasp. This simulation will iteratively close the fingers towards the center of the object, evaluate the forces transmitted to the object by solving the contact model, update the state of the contact surface due to deformations, and verify the static equilibrium of the hand + object system. When this static equilibrium is obtained in the simulation, the contact forces applied by the simulated fingers will be used as references for the force control of the real robotic hand. An example of this grasping execution strategy will be shown in Section 7 in order to justify its application in our pipeline. Nevertheless, more experiments of this grasp execution strategy can be found in the previous work [33] by the authors, where it was first proposed.

7. Experimental Validation of the Grasp Planning Pipeline for the Hand + Arm System

The different steps of our complete grasp planning pipeline are validated with simulation and real experiments. First of all, the synthesis algorithm for the first initial grasp configuration proposed in Section 3 (i.e., Algorithm 1) is validated for three different shapes: a sphere, a cylinder, and a cube (Figure 10). This algorithm has been implemented in Matlab, by integrating a discrete 3D tetrahedral representation of the shape of these objects. The number of nodes of this 3D representation and the values of the two grasping quality metrics computed by the algorithm for the three objects are shown in Table 1. The initial grasping points obtained are shown in Figure 10 and they do not consider any deformation of the objects.

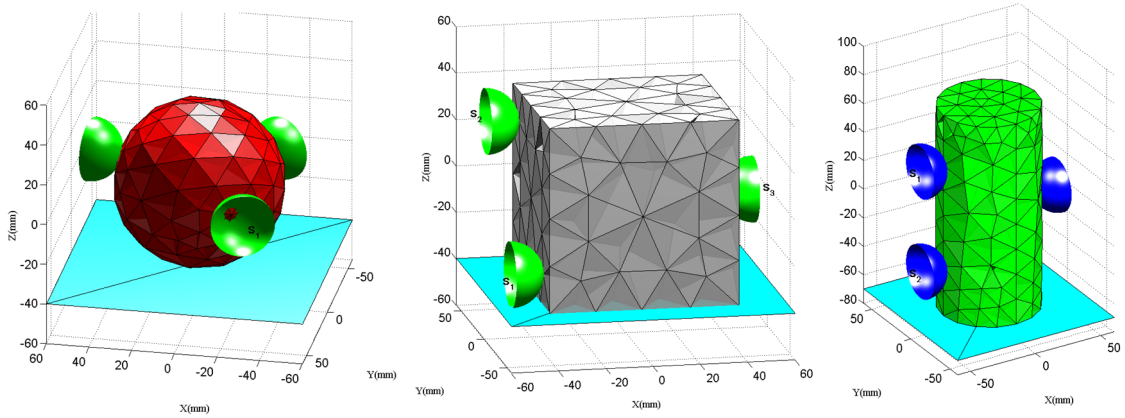

Figure 10. Configuration of the initial grasping points for a sphere, a cube, and a cylinder.

Table 1. Evaluation of the initial grasping criteria for a sphere, a cube, and a cylinder.

	Sphere (80 mm)	Cube (80∗80∗80mm)	Cylinder (R35mm∗L140 mm)
Number of nodes	182	162	226
Q1	0.0491	0.2302	0.1145
Q2 (mm)	4.8659	13.334	11.6667

These initial grasp configurations are used as input for the pregrasp and grasp execution steps of the grasp planning pipeline. For validating both steps, real experiments with the Adept arm and the Barrett hand grasping a foam cube (Figure 11) and a cylinder (Figure 12) are performed. Both objects represent typical shapes found in grasping applications of industrial products: a planar-faced surface (e.g., a cube) and a revolution surface (e.g., a cylinder). After the grasping, the object is lifted and carried to another position over the table in order to validate the stability of the grasp. The first step consists of generating and executing the path of the Adept arm for the pregrasp configuration in simulation, ensuring that the object is within the Barrett hand workspace (as explained for the cube in

Figure 9a–c). The trajectory of the arm and the closing of the hand are then performed in the simulation (Figure 9d) until the fingers come into contact with the object.

The second step is to model the interaction between the fingers and the object for closing the fingers against the object surface in order to get the required contact forces in simulation (as explained in Section 6). The real contact forces at each finger are obtained by strain gauges installed in the phalanxes of the Barrett hand. Thereby, the Barrett hand is iteratively closed until the contact forces obtained from the simulation of the contact model are attained (as shown in Figure 13). Thus, a stable final grasp of the deformable object is obtained and the object can be lifted without any danger of falling down. Figure 13 shows the variation in the norm of the three forces applied to the cube during the simulation of the contact model. At the initial step (t_0) of the simulation, the fingers move towards the object in order to reach the initial contact points. When the fingers come into contact with the object (t_1), the contact model starts to evaluate the applied forces. This figure also shows that the contact forces are continuous and directly related to the amount of local deformation inside the contact area. The fingers continue to apply forces until equilibrium conditions are satisfied (i.e., reaching the three fingers' contact forces thresholds, identified by horizontal dashed lines in Figure 13). Once this state is reached and the three force thresholds are obtained, the fingers should keep these contact forces in order to ensure stable handling and then the simulation can stop.

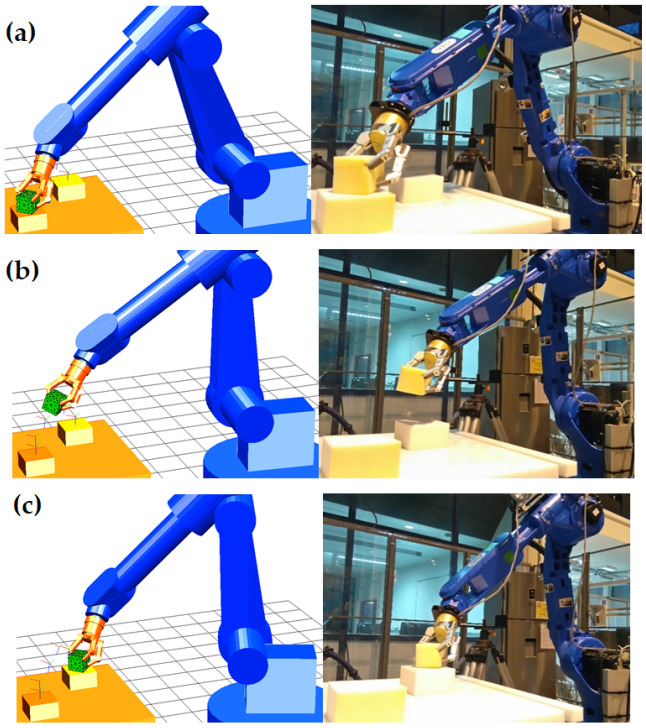

Figure 11. Pick-and-place of the cube by the Adept robot and the Barrett hand: (**a**) grasping, (**b**) lifting, and (**c**) leaving.

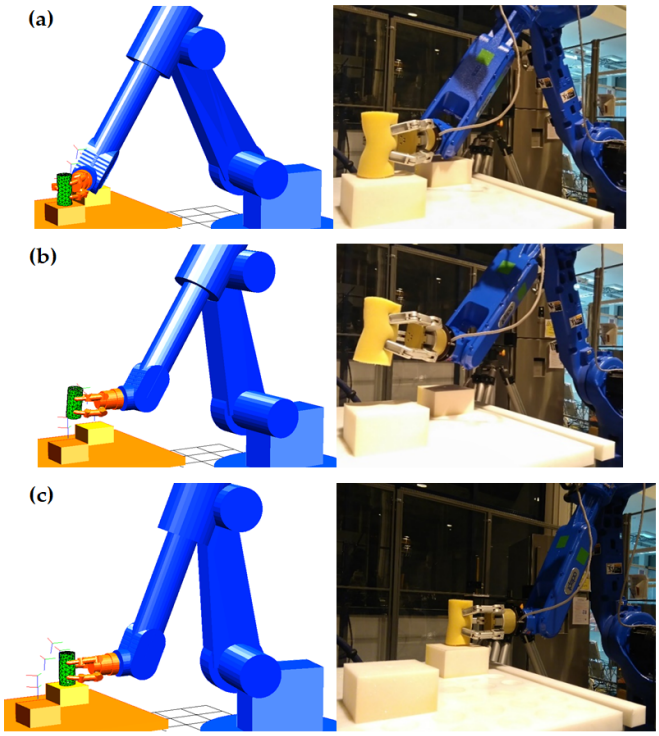

Figure 12. Pick-and-place of a cylinder by the Adept robot and the Barrett hand: (**a**) grasping, (**b**) lifting, and (**c**) leaving.

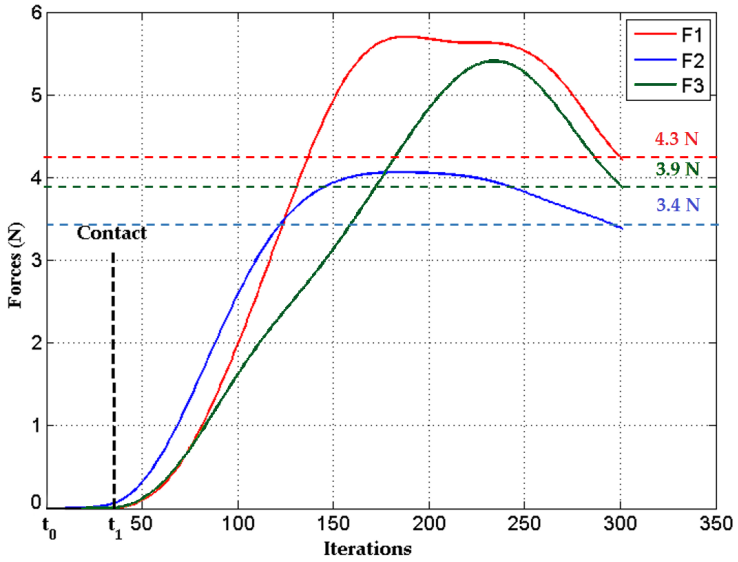

Figure 13. Grasping forces applied by the three fingers of the Barrett hand (F1, F2 and F3) in simulation.

The relation between these force thresholds and penetration of the fingers inside the object (i.e., the deformation of its surface) is obtained by the simulation of the contact interaction model while closing the fingertips over the object. The real relation force–penetration is very similar to the one computed in the simulation (see real validation experiments in [33]). Thereby, our strategy of applying the contact forces obtained from simulation in real grasping is suitable. In fact, the mean error of the contact force obtained by our model is of $0.3N$, which implies that only 15% of typical contact forces is required for grasping most common life deformable objects. In addition, the nonlinear relation force–penetration shows that simplified linear models cannot be used for grasping significantly deformable objects and justifies the necessity of the proposed model. The proposed grasp planning

strategy is validated by the correct execution of two pick-and-place tasks (for a cube and a cylinder): lifting and stable transportation of both objects with the real robot without any slippage (as shown in the real photographs of Figures 11 and 12).

8. Conclusions

This work has been devoted to the complete process of deformable object grasp planning with an industrial manipulator (robotic hand + robotic arm). First of all, this requires the definition of the grasp points over the surface of the object and thus, the determination of an initial grasp configuration. Later, we presented our approach for determining the pregrasp strategy for reaching this initial grasp by taking into account the kinematic constraints of the arm and the hand. Thereby, the grasp planning has been divided into two phases: firstly, determining the configuration of the robot arm to bring the hand close to the object; secondly, determining the appropriate configuration of the fingers of the hand to grasp the object. The determination of the joint parameters of the arm and the hand is ensured by the resolution of their inverse kinematics. In the case of the hand, the implemented strategy consists first of putting the TCP (line perpendicular to the palm of the hand) at an intersection with the center of the grasp triangle (obtained in the initial grasp synthesis) and aligning it with the normal vector of this grasp triangle. The second step is to iteratively search for a solution to the articular parameters of the three fingers of the Barrett hand in order to bring them into correspondence with the grasping points previously defined by force-closure-type stability conditions. Thereby, this final grasp solution combines the initial grasp based on a general geometric criteria for force closure (i.e., it only considers the shape of the object) with the kinematic constraints of the robotic hand by applying the proposed pregrasp strategy. Nevertheless, this grasp configuration does guarantee the robustness of the grasp only for rigid objects but not for deformable objects. Thus, a force–deformation serving scheme is activated when the fingers come into contact with the deformable object to be grasped. This scheme is based on a simulation of the object–fingers interaction (previously developed by the authors in [33]), which obtains the contact force thresholds that should be applied by the fingers in order to guarantee a stable grasp while deforming the surface of the object. Finally, an iterative closing of the real fingers is performed in order to attain these contact forces with the real object.

Objects with simple geometrical shapes (sphere, cube, and cylinder) were chosen for the experiments to more efficiently simulate the interaction model described in Section 6. The proposed pregrasp/grasp pipeline is not restricted to simple shapes and can be applied to any shape of object. In fact, the mesh construction process required by the interaction model has been applied by the authors to very irregular shapes of meat pieces in a previous work [10]. This grasp planning pipeline is designed for nonlinear deformable objects to be manipulated by three-fingered robotic hands, but its architecture could be redesigned as a group of interchangeable modules in future works. These modules could include the following: other types of objects (e.g., changing the contact interaction model for rigid objects, granular media [53]), new sensing data (i.e., combining tactile and vision information for estimating the 3D shape of the object and the real contact forces in real-time [54]), multiple robotic fingers (e.g., dexterous robotic hands [55]), or even more complex manipulation tasks (e.g., in-hand manipulation [56]).

Author Contributions: Conceptualization, Methodology: all authors; Software: L.Z., J.A.C.R., L.S. and B.C.B.; Validation: L.Z. and L.S.; Writing – original draft: L.Z.; Writing – review & editing: L.Z and J.A.C.R.

Funding: This work has received funding from the European Union's Horizon 2020 research and innovation programme under grant agreement nº 869855 (Project 'SoftManBot').

Acknowledgments: L.Z. thanks the research support by the LINEACT EA 7527 laboratory at CESI Rouen.

Conflicts of Interest: The authors declare no conflicts of interest.

References

1. Sahbani, A.; El-Khoury, S.; Bidaud, P. An overview of 3D object grasp synthesis algorithms. *Robot. Auton. Syst.* **2012**, *60*, 326–336.
2. Ramón, J.A.C.; Medina, F.T.; Perdereau, V. Finger readjustment algorithm for object manipulation based on tactile information. *Int. J. Adv. Robot. Syst.* **2013**, *10*, 9.
3. Adjigble, M.; Marturi, N.; Ortenzi, V.; Rajasekaran, V.; Corke, P.; Stolkin, R. Model-free and learning-free grasping by local contact moment matching. In Proceedings of the 2018 IEEE/RSJ International Conference on Intelligent Robots and Systems (IROS), Madrid, Spain, 1–5 October 2018; pp. 2933–2940.
4. Mavrakis, N.; Stolkin, R. Estimation and exploitation of objects' inertial parameters in robotic grasping and manipulation: A survey. *Robot. Auton. Syst.* **2020**, *124*, 103374.
5. Wang, C.; Zhang, X.; Zang, X.; Liu, Y.; Ding, G.; Yin, W.; Zhao, J. Feature Sensing and Robotic Grasping of Objects with Uncertain Information: A Review. *Sensors* **2020**, *20*, 3707.
6. Deng, Z.; Jonetzko, Y.; Zhang, L.; Zhang, J. Grasping Force Control of Multi-Fingered Robotic Hands through Tactile Sensing for Object Stabilization. *Sensors* **2020**, *20*, 1050.
7. Oravcová, J.; Košťál, P.; Delgado Sobrino, D.R.; Holubek, R. Clamping Fixture Design Methodology for the Proper Workpiece Insertion. In *III Central European Conference on Logistics, Applied Mechanics and Materials*;Trans Tech Publications Ltd.: Switzerland,2013; Volume 309, pp. 20–26, doi:10.4028/www.scientific.net/AMM.309.20.
8. Velíšek, K.; Košťál, P.; Zvolenský, R. Clamping Fixtures for Intelligent Cell Manufacturing. In *Intelligent Robotics and Applications*; Xiong, C., Liu, H., Huang, Y., Xiong, Y., Eds.; Springer Berlin Heidelberg: Berlin, Heidelberg, Germany, 2008; pp. 966–972.
9. Faure, F.; Duriez, C.; Delingette, H.; Allard, J.; Gilles, B.; Marchesseau, S.; Talbot, H.; Courtecuisse, H.; Bousquet, G.; Peterlik, I.; et al. Sofa: A multi-model framework for interactive physical simulation. In *Soft Tissue Biomechanical Modeling for Computer Assisted Surgery*; Springer: Berlin, Heidelberg, Germany,2012; pp. 283–321.
10. Long, P.; Khalil, W.; Martinet, P. Force/vision control for robotic cutting of soft materials. In Proceedings of the 2014 IEEE/RSJ International Conference on Intelligent Robots and Systems, Chicago, IL, USA, 14–18 September 2014; pp. 4716–4721.
11. Nabil, E.; Belhassen-Chedli, B.; Grigore, G. Soft material modeling for robotic task formulation and control in the muscle separation process. *Robot. Comput.-Integr. Manuf.* **2015**, *32*, 37–53.
12. Nadon, F.; Valencia, A.J.; Payeur, P. Multi-modal sensing and robotic manipulation of non-rigid objects: A survey. *Robotics* **2018**, *7*, 74.
13. Pirník, R.; Hruboš, M.; Nemec, D.; Mravec, T.; Božek, P. Integration of Inertial Sensor Data into Control of the Mobile Platform. In *Advances in Intelligent Systems and Computing, Proceedings of the 2015 Federated Conference on Software Development and Object Technologies, Žilina, Slovakia, 19–20 November 2017*; Janech, J., Kostolny, J., Gratkowski, T., Eds.; Springer International Publishing: Cham, Switzerland, 2017; pp. 271–282.
14. Dodok, T.; Čuboňová, N.; Císar, M.; Kuric, I.; Zajačko, I. Utilization of Strategies to Generate and Optimize Machining Sequences in CAD/CAM. *Procedia Eng.* **2017**, *192*, 113–118. 12th international scientific conference of young scientists on sustainable, modern and safe transport, doi:10.1016/j.proeng.2017.06.020.
15. Sanchez, J.; Corrales, J.A.; Bouzgarrou, B.C.; Mezouar, Y. Robotic manipulation and sensing of deformable objects in domestic and industrial applications: A survey. *Int. J. Robot. Res.* **2018**, *37*, 688–716.
16. Chinellato, E.; Morales, A.; Fisher, R.B.; Del Pobil, A.P. Visual quality measures for characterizing planar robot grasps. *Syst. Man Cybern. Part C Appl. Rev. IEEE Trans.* **2005**, *35*, 30–41.
17. Roa, M.A.; Suárez, R. Grasp quality measures: Review and performance. *Auton. Robot.* **2015**, *38*, 65–88.
18. Pozzi, M.; Malvezzi, M.; Prattichizzo, D. On grasp quality measures: Grasp robustness and contact force distribution in underactuated and compliant robotic hands. *IEEE Robot. Autom. Lett.* **2016**, *2*, 329–336.
19. Soler, F.; Rojas-de Silva, A.; Suárez, R. Grasp quality measures for transferring objects. In *Advances in Intelligent Systems and Computing, Proceedings of the Iberian Robotics Conference, Seville, Spain, 22–24 November 2017*; Springer: Cham, Switzerland, 2017; pp. 28–39.
20. Wakamatsu, H.; Hirai, S.; Iwata, K. Static analysis of deformable object grasping based on bounded force closure. In Proceedings of the EEE International Conference on Robotics and Automation, Minneapolis, MN, USA, 22–28 April 1996; Volume 4, pp. 3324–3329.

21. Mira, D.; Delgado, A.; Mateo, C.; Puente, S.; Candelas, F.; Torres, F. Study of dexterous robotic grasping for deformable objects manipulation. In Proceedings of the 2015 23rd Mediterranean Conference on Control and Automation (MED), Torremolinos, Spain, 16–19 June 2015; pp. 262–266.
22. Xu, J.; Danielczuk, M.; Ichnowski, J.; Mahler, J.; Steinbach, E.; Goldberg, K. Minimal Work: A Grasp Quality Metric for Deformable Hollow Objects. In Proceedings of the 2020 IEEE International Conference on Robotics and Automation (ICRA), Paris, France, 31 May–31 August 2020; pp. 1546–1552.
23. Jørgensen, T.B.; Jensen, S.H.N.; Aanæs, H.; Hansen, N.W.; Krüger, N. An adaptive robotic system for doing pick and place operations with deformable objects. *J. Intell. Robot. Syst.* **2019**, *94*, 81–100.
24. Bicchi, A. On the closure properties of robotic grasping. *Int. J. Robot. Res.* **1995**, *14*, 319–334.
25. Lei, Q.; Wisse, M. Object grasping by combining caging and force closure. In Proceedings of the 2016 14th International Conference on Control, Automation, Robotics and Vision (ICARCV), Phuket, Thailand, 13–15 November 2016; pp. 1–8.
26. Rakesh, V.; Sharma, U.; Murugan, S.; Venugopal, S.; Asokan, T. Optimizing force closure grasps on 3D objects using a modified genetic algorithm. *Soft Comput.* **2018**, *22*, 759–772.
27. Kaboli, M.; Yao, K.; Cheng, G. Tactile-based manipulation of deformable objects with dynamic center of mass. In Proceedings of the 2016 IEEE-RAS 16th International Conference on Humanoid Robots (Humanoids), Cancun, Mexico, 15–17 November 2016; pp. 752–757.
28. Zhao, K.; Li, X.; Lu, C.; Lu, G.; Wang, Y. Video-based slip sensor for multidimensional information detecting in deformable object grasp. *Robot. Auton. Syst.* **2017**, *91*, 71–82.
29. Gonthier, Y.; McPhee, J.; Lange, C.; Piedboeuf, J.C. A regularized contact model with asymmetric damping and dwell-time dependent friction. *Multibody Syst. Dyn.* **2004**, *11*, 209–233.
30. Dopico, D.; Luaces, A.; Gonzalez, M.; Cuadrado, J. Dealing with multiple contacts in a human-in-the-loop application. *Multibody Syst. Dyn.* **2011**, *25*, 167–183.
31. Mohammadi, M.; Baldi, T.L.; Scheggi, S.; Prattichizzo, D. Fingertip force estimation via inertial and magnetic sensors in deformable object manipulation. In Proceedings of the 2016 IEEE Haptics Symposium (HAPTICS), Philadelphia, PA, USA, 8–11 April 2016; pp. 284–289.
32. Lu, Z.; Huang, P.; Liu, Z. High-gain nonlinear observer-based impedance control for deformable object cooperative teleoperation with nonlinear contact model. *Int. J. Robust Nonlinear Control* **2020**, *30*, 1329–1350.
33. Zaidi, L.; Corrales, J.A.; Bouzgarrou, B.C.; Mezouar, Y.; Sabourin, L. Model-based strategy for grasping 3D deformable objects using a multi-fingered robotic hand. *Robot. Auton. Syst.* **2017**, *95*, 196–206.
34. Arriola-Rios, V.E.; Guler, P.; Ficuciello, F.; Kragic, D.; Siciliano, B.; Wyatt, J.L. Modeling of Deformable Objects for Robotic Manipulation: A Tutorial and Review. *Front. Robot. AI* **2020**, *7*, 82, doi:10.3389/frobt.2020.00082.
35. Hammer, P.E.; Sacks, M.S.; Pedro, J.; Howe, R.D. Mass-spring model for simulation of heart valve tissue mechanical behavior. *Ann. Biomed. Eng.* **2011**, *39*, 1668–1679.
36. Jarrousse, O. *Modified Mass-Spring System for Physically Based Deformation Modeling*; KIT Scientific Publishing: Karlsruhe, Germany, 2014.
37. Garg, S.; Dutta, A. Grasping and manipulation of deformable objects based on internal force requirements. *Int. J. Adv. Robot. Syst.* **2006**, *3*, 107–114.
38. Han, L.; Hipwell, J.; Taylor, Z.; Tanner, C.; Ourselin, S.; Hawkes, D.J. Fast deformation simulation of breasts using GPU-based dynamic explicit finite element method. In *Digital Mammography*; Springer: Berlin, Heidelberg, Germany,2010; pp. 728–735.
39. Tagawa, K.; Hirota, K.; Hirose, M. *Manipulation of Dynamically Deformable Object Using Impulse-Based Approach*;INTECH Open Access Publisher: London, United Kingdom, 2010.
40. Zaidi, L.; Bouzgarrou, B.C.; Sabourin, L.; Mezouar, Y. Modeling and analysis of 3D deformable object grasping. In Proceedings of the 2014 23rd International Conference on Robotics in Alpe-Adria-Danube Region (RAAD), Smolenice, Slovakia, 3–5 September 2014; pp. 1–8, doi:10.1109/RAAD.2014.7002259.
41. Berenson, D. Manipulation of deformable objects without modeling and simulating deformation. In Proceedings of the 2013 IEEE/RSJ International Conference on Intelligent Robots and Systems, Tokyo, Japan, 3–7 November 2013; pp. 4525–4532, doi:10.1109/IROS.2013.6697007.
42. Nadon, F.; Payeur, P. Automatic Selection of Grasping Points for Shape Control of Non-Rigid Objects. In Proceedings of the 2019 IEEE International Symposium on Robotic and Sensors Environments (ROSE), Ottawa, ON, Canada, 17–18 June 2019; pp. 1–7.

43. Jia, Y.B.; Guo, F.; Lin, H. Grasping deformable planar objects: Squeeze, stick/slip analysis, and energy-based optimalities. *Int. J. Robot. Res.* **2014**, *33*, 866–897.
44. Sanchez, J.; Mohy El Dine, K.; Corrales, J.A.; Bouzgarrou, B.C.; Mezouar, Y. Blind Manipulation of Deformable Objects Based on Force Sensing and Finite Element Modeling. *Front. Robot. AI* **2020**, *7*, 73, doi:10.3389/frobt.2020.00073.
45. Lin, H.; Guo, F.; Wang, F.; Jia, Y.B. Picking up a soft 3D object by feeling the grip. *Int. J. Robot. Res.* **2015**, *34*, 1361–1384, doi:10.1177/0278364914564232.
46. Jorgensen, T.B.; Holm, P.H.S.; Petersen, H.G.; Krüger, N. Optimizing Pick and Place Operations in a Simulated Work Cell For Deformable 3D Objects. In *Lecture Notes in Computer Science, Proceedings of the International Conference on Intelligent Robotics and Applications, Portsmouth, UK, 24–27 August 2015*; Springer: Cham, Switzerland, 2015; pp. 431–444.
47. Hu, Z.; Sun, P.; Pan, J. Three-Dimensional Deformable Object Manipulation Using Fast Online Gaussian Process Regression. *IEEE Robot. Autom. Lett.* **2018**, *3*, 979–986, doi:10.1109/LRA.2018.2793339.
48. Verleysen, A.; Holvoet, T.; Proesmans, R.; Den Haese, C.; wyffels, F. Simpler Learning of Robotic Manipulation of Clothing by Utilizing DIY Smart Textile Technology. *Appl. Sci.* **2020**, *10*, 4088, doi:10.3390/app10124088.
49. Caporali, A.; Palli, G. Pointcloud-based Identification of Optimal Grasping Poses for Cloth-like Deformable Objects. In Proceedings of the 2020 25th IEEE International Conference on Emerging Technologies and Factory Automation (ETFA), Vienna, Austria, 8–11 September 2020; Volume 1, pp. 581–586.
50. Hasan, M.R.; Vepa, R.; Shaheed, H.; Huijberts, H. Modelling and Control of the Barrett Hand for Grasping. In Proceedings of the 2013 UKSim 15th International Conference on Computer Modelling and Simulation, Cambridge, UK, 10–12 April 2013; pp. 230–235, doi:10.1109/UKSim.2013.142.
51. Shi, X.; Polycarpou, A.A. Measurement and modeling of normal contact stiffness and contact damping at the meso scale. *J. Vib. Acoust.* **2005**, *127*, 52–60.
52. Johnson, K.L.; Johnson, K.L. *Contact Mechanics*; Cambridge University Press: Cambridge, UK, 1987.
53. Mateo, C.M.; Corrales, J.A.; Mezouar, Y. A Manipulation Control Strategy for Granular Materials Based on a Gaussian Mixture Model. In *Advances in Intelligent Systems and Computing, Proceedings of the Robot 2019: Fourth Iberian Robotics Conference, Porto, Portugal, 20–22 November 2019*; Silva, M.F., Luís Lima, J., Reis, L.P., Sanfeliu, A., Tardioli, D., Eds.; Springer International Publishing: Cham, Switzerland, 2020; pp. 171–183.
54. Sanchez, J.; Mateo, C.M.; Corrales, J.A.; Bouzgarrou, B.; Mezouar, Y. Online Shape Estimation based on Tactile Sensing and Deformation Modeling for Robot Manipulation. In Proceedings of the 2018 IEEE/RSJ International Conference on Intelligent Robots and Systems (IROS), Madrid, Spain, 1–5 October 2018; pp. 504–511, doi:10.1109/IROS.2018.8594314.
55. Aranda, M.; Corrales, J.A.; Mezouar, Y. Deformation-based shape control with a multirobot system. In Proceedings of the 2019 International Conference on Robotics and Automation (ICRA), Montreal, QC, Canada, 20–24 May 2019; pp. 2174–2180, doi:10.1109/ICRA.2019.8793811.
56. Corrales Ramón, J.A.; Perdereau, V.; Torres Medina, F. Multi-fingered robotic hand planner for object reconfiguration through a rolling contact evolution model. In Proceedings of the 2013 IEEE International Conference on Robotics and Automation, Karlsruhe, Germany, 6–10 May 2013; pp. 625–630, doi:10.1109/ICRA.2013.6630638.